

# Linear and non-linear AVO for poroelastic targets

Steven Kim, Kris Innanen

## ABSTRACT

AVO techniques permit the variations in seismic amplitudes with angle or offset to be used to deduce subsurface target properties. Linearized AVO is parameterized in several different ways. One, introduced this year focuses on changes in the P-wave reflection strength associated with poroelastic medium variations. In this paper we review a newly proposed poroelastic AVO technique, and reproduce the methodology and basic conclusions of those authors. We formulate the poroelastic AVO inverse problem in terms of least-squares, and take some initial steps towards extending the model to nonlinear (i.e., large contrast) regimes.

## INTRODUCTION

AVO analysis allows our ability to infer lithological and fluid properties of the subsurface given the behaviour of the amplitude information in the seismic. Russell et al. (2011) presents an accessible and straightforward-to-implementation alteration of classic AVO theory to this end. The goals of this paper are to (a) review AVO theory through the exact and linearized AVO approximations, (b) reproduce the results provided by Russell et al. (2011), and (c) examine the linear inverse problem and to identify a possible avenue of extension. But first we shall introduce poroelasticity theory as proposed by Biot (1941) and Gassmann (1951) which essentially accounts for the presence of fluid within a dry rock frame.

## THEORY

### I. Poroelasticity

Poroelasticity theory concerns what happens when we introduce a pore fluid into an initially dry (or drained) porous rock (Russell et al., 2011). Since elastic material behaves in a way such that a geological model assumes homogeneity and isotropy, poroelasticity theory further extends how porosity and fluids affect the physical properties of the medium of interest. These physical properties then affect the amplitude of a travelling wavefield that interacts with that medium. Through the works of Biot (1941) and Gassmann (1951), Berryman (1999) shows a stress and strain relationship which can be seen in equation (1)

$$\begin{bmatrix} e_{11} \\ e_{22} \\ e_{33} \\ \zeta \end{bmatrix} = \begin{bmatrix} s_{11}^{dry} & s_{12}^{dry} & s_{12}^{dry} & \beta \\ s_{12}^{dry} & s_{11}^{dry} & s_{12}^{dry} & \beta \\ s_{12}^{dry} & s_{12}^{dry} & s_{11}^{dry} & \beta \\ \beta & \beta & \beta & -\gamma \end{bmatrix} \begin{bmatrix} \sigma_{11} \\ \sigma_{22} \\ \sigma_{33} \\ p_f \end{bmatrix} \quad (1)$$

where the  $s_{**}^{dry}$  values represent undrained or dry compliances,  $e_{**}$  represent strain,  $\sigma_{**}$  represent stress, and  $\beta$  and  $\gamma$  represent two physical constants. The  $\zeta$  term measures how much of the original fluid in the pores is squeezed out during the compression of the pore volume while including the effects of compression or expansion of the pore fluid itself due

to changes in  $p_f$  where it can be shown that the dry compliances can be solved by setting  $\zeta = 0$ . The undrained compliances can be written in terms of Lamé parameters, bulk modulus, shear modulus, Young's modulus and Poisson's ratio. This is shown by

$$s_{11}^{dry} = \frac{1}{E_{dry}} = \frac{\lambda_{dry} + \mu_{dry}}{\mu_{dry}(\lambda_{dry} + 2\mu_{dry})} = \frac{1}{9\kappa_{dry}} + \frac{1}{3\mu_{dry}} \quad (2)$$

and

$$s_{12}^{dry} = -\frac{\nu}{E_{dry}} = \frac{\lambda_{dry}}{2\mu_{dry}(3\lambda_{dry} + 2\mu_{dry})} = \frac{1}{9\kappa_{dry}} + \frac{1}{6\mu_{dry}}. \quad (3)$$

Since Berryman (1999) is dealing with an isotropic model, seven poroelastic equations and seven unknowns have been reduced to four poroelastic equations with four unknowns which is shown in equation (1) (Russell et al., 2011). By assuming that there is no change in pore fluid mass, an expression to solve equation (1) for the saturated compliances is shown by Berryman (1999) which is done by inverting the matrix of dry compliances which will then give you a matrix of dry stiffnesses. But without going into much detail, we can draw two important conclusions from what we have seen so far (Russell et al., 2011). The first conclusion is noting that there is a relation between equation (1) and (4) where Biot (1941) shows that  $c_{ij}^{sat} = c_{ij}^{dry} + \alpha^2 M$  where the inverted matrix of dry stiffnesses is replaced with saturated stiffnesses using this equation. This is shown below in equation (4) where

$$\begin{bmatrix} \sigma_{11} \\ \sigma_{22} \\ \sigma_{33} \\ p_f \end{bmatrix} = \begin{bmatrix} c_{11}^{sat} & c_{12}^{sat} & c_{12}^{sat} & -\alpha M \\ c_{12}^{sat} & c_{11}^{sat} & c_{12}^{sat} & -\alpha M \\ c_{12}^{sat} & c_{12}^{sat} & c_{11}^{sat} & -\alpha M \\ -\alpha M & -\alpha M & -\alpha M & M \end{bmatrix} \begin{bmatrix} e_{11} \\ e_{22} \\ e_{33} \\ \zeta \end{bmatrix}. \quad (4)$$

The second conclusion involves the expressions for the dry stiffnesses where they are written similarly like the dry compliances where

$$c_{11}^{dry} = \lambda_{dry} + 2\mu_{dry} = \kappa_{dry} + \frac{4}{3}\mu_{dry} \quad (5)$$

and

$$c_{12}^{dry} = \lambda_{dry} = \kappa_{dry} - \frac{2}{3}\mu_{dry}. \quad (6)$$

So by using both conclusions, we can find that

$$c_{11}^{sat} - c_{12}^{sat} = c_{11}^{dry} - c_{12}^{dry} \quad (7)$$

is true and we can cancel the  $\alpha^2 M$  terms and see that

$$\mu_{sat} = \mu_{dry}. \quad (8)$$

Equation (8) implies that the pore fluid does not affect the shear rigidity. Russell et al. (2011) states that with equation (8), the  $\mu$  terms can be canceled when equating the dry and saturated stiffness terms as shown in equation (7) where

$$\lambda_{sat} = \lambda_{dry} + \alpha^2 M \quad (9)$$

and

$$\kappa_{sat} = \kappa_{dry} + \alpha^2 M. \quad (10)$$

The  $\alpha^2 M$  terms are what is known as the fluid term that shows a relation between the drained and undrained parameters as shown above. Gassmann (1951) derives those parameters in terms of elastic constants where

$$\alpha = 1 - \frac{\kappa_{dry}}{\kappa_m} \quad (11)$$

$$\frac{1}{M} = \frac{\alpha - \phi}{\kappa_m} + \frac{\phi}{\kappa_{fl}}. \quad (12)$$

The  $\alpha$  term acts as a control which determines the amount of fluid that is inside a dry rock frame. If the rock frame is entirely fluid free,  $\kappa_{dry}/\kappa_m$  is one and  $\alpha$  then disappears in equations (9) and (10). This provides an extra control variable that can be used to calculate  $(V_P)_{sat}$  and  $(V_S)_{sat}$  as shown by Russell et al. (2011).

## II. AVO modelling, linear approximation

From the Zoeppritz equations, several linear approximations have been derived. With these approximations, we can model AVO curves along with the Zoeppritz curve for comparison. As shown below, these linearized approximations plotted alongside Zoeppritz provide very similar results for small angles of incidence. As the angle of incidence increases, the differences between these approximations versus the exact expressions increases. The different approximations, although produce similar reflection coefficients to one another, each linearly approximated AVO expression is derived using different medium parameters. For instance, Aki and Richards (2002) require the compressional and shear wave velocities as well as the densities to calculate the reflection coefficient of a particular angle. Similarly, Shuey (1985) derives an approximation using the same inputs as Aki and Richards (2002) however, uses poisson's ratio instead of density. These expressions will be explained in more detail in the next section as well as show an expression derived by Russell et al. (2011). Although AVO analysis does help us provide some insight into the fluid content of a medium of interest, Russell et al. (2011) derives an expression that directly inverts for a fluid term in the AVO equation itself.

### LINEAR POROELASTIC AVO

As an incident P-wave travels towards a boundary at normal incidence, a transmitted and reflected P-wave is generated. If the incident P-wave travels at an angle towards the boundary, then a mode conversion will occur in which transmitted and reflected P- and S-waves will be generated on both sides of the boundary (Russell et al., 2011). This is shown in figure 1. The amplitudes of the travelling waves can be characterized by the Zoeppritz equations which determine seismic amplitude responses at the surface at different offsets.

Ostrander (1984) became familiar with this type of behaviour and adapted the notion that these AVO responses were mainly characterized by the Poisson's ratio of two different media of a given interface. Other parameterizations of AVO curves can also be forward modelled in terms of  $V_P$ ,  $V_S$ , and  $\rho$  where Aki and Richards (2002) have derived an equation where the incident and reflected P-wave amplitude is written as

$$R_{PP}(\theta) = (1 + \tan^2\theta) \frac{\Delta V_P}{2V_P} + \left( \frac{-8\sin^2\theta}{\gamma_{sat}^2} \right) \frac{\Delta V_S}{2V_S} + \left( 1 - \frac{4\sin^2\theta}{\gamma_{sat}^2} \right) \frac{\Delta\rho}{2\rho} \quad (13)$$

where  $\gamma_{sat}$  is a  $V_P/V_S$  ratio for a fluid saturated medium and the notation used here was adapted from Russell et al. (2011). Each reflectivity term in the equation above is characterized by a forward modelled P-wave velocity, S-wave velocity and density. Each term in the denominator of the three linear terms in equation (13), display the average  $V_P$ ,  $V_S$ , and  $\rho$  between the media of interest. The terms in the numerator are simply the differences of each corresponding elastic parameter. Accompanying each reflectivity term is a weighting term that is a function of incidence angle. This equation is a linearized approximation to the Zoeppritz equations. Although it would be ideal to use the full Zoeppritz equations in order to invert for physical properties of the Earth, the nonlinear schemes may be unstable (Russell et al., 2011). For AVO analysis, the near offsets are used rather than the farther offsets as far offset data are subjected to greater error in the AVO amplitude estimation. This greater error can be seen in the  $\Delta$  terms of equation (13) where the ratios for  $V_P$ ,  $V_S$ , and  $\rho$  cannot be large (Russell et al., 2011).

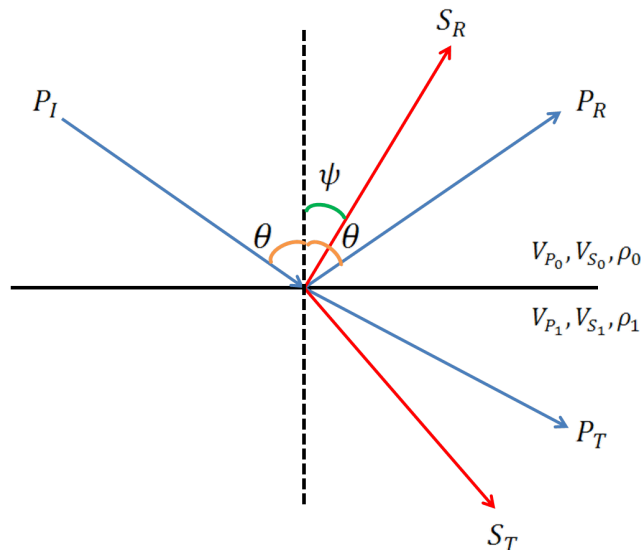


FIG. 1: An incident P-wave approaching a boundary at an angle  $\theta$  where P- and S-wave reflections and transmissions are produced. The medium properties being analyzed in the forward modelling involves a P-wave ( $V_P$ ), S-wave ( $V_S$ ), and density ( $\rho$ ).

Amplitude estimates from equation (13) seem to be adequate for small offsets when compared to the Zoeppritz values. There are a handful of AVO approximations that have been derived that also produce similar results to Aki and Richards (2002) such as Shuey's approximation where the three forward modelled terms are of P-wave velocity, density, and Poisson's ratio. Gray et al. (1999) also derives, not one, but two expressions for AVO which

are written in terms of  $\lambda$ ,  $\mu$ ,  $\rho$ , and  $\kappa$ ,  $\mu$ ,  $\rho$  respectively. All of these expressions to predict AVO are similar for elastic constant media. Russell et al. (2011) shows however, that an expression for AVO which includes the combined works of Biot (1941) and Gassmann (1951) can be useful for fluid filled layers. Using poroelasticity theory, Russell et al. (2011) applies both fluid and rock matrix properties to determine an approximated wave amplitude signature. The equation that was derived by Russell et al. (2011) is a function of a fluid term,  $f$ , a saturated shear modulus,  $\mu$ , and a saturated density,  $\rho$  where

$$R_{PP}(\theta) = \left[ \left( 1 - \frac{\gamma_{dry}^2}{\gamma_{sat}^2} \right) \frac{\sec^2\theta}{4} \right] \frac{\Delta f}{f} + \left[ \frac{\gamma_{dry}^2}{4\gamma_{sat}^2} \sec^2\theta - \frac{2}{\gamma_{sat}^2} \sin^2\theta \right] \frac{\Delta\mu}{\mu} + \left[ \frac{1}{2} - \frac{\sec^2\theta}{4} \right] \frac{\Delta\rho}{\rho} \quad (14)$$

The way in which this formula was derived was by incorporating poroelasticity with the two formulations provided by Gray et al. (1999) into one single equation. This equation is referred to as the  $f - m - r$  (fluid-mu-rho) equation.

Because equation (14) is a linear sum of three reflectivity terms, it can be used to extract estimates of the three reflectivities from seismic (Russell et al., 2011). This can be written in the form of

$$\begin{bmatrix} R_{PP}(\theta_1) \\ R_{PP}(\theta_2) \\ \vdots \\ R_{PP}(\theta_N) \end{bmatrix} = \begin{bmatrix} c_1(\theta_1) & c_2(\theta_1) & c_3(\theta_1) \\ c_1(\theta_2) & c_2(\theta_2) & c_3(\theta_2) \\ \vdots & \vdots & \vdots \\ c_1(\theta_N) & c_2(\theta_N) & c_3(\theta_N) \end{bmatrix} \begin{bmatrix} \frac{\Delta f}{f} \\ \frac{\Delta\mu}{\mu} \\ \frac{\Delta\rho}{\rho} \end{bmatrix} \quad (15)$$

where  $c_i(\theta_j)$  represents the weighting terms in front of each poroelastic term.

Since this type of expression is known as an overdetermined system, there are many more data points,  $R_{PP}(\theta)$ , then there are unknown variables to solve for. Here we have only three unknown parameters which are  $\frac{\Delta f}{f}$ ,  $\frac{\Delta\mu}{\mu}$ , and  $\frac{\Delta\rho}{\rho}$ . Our data points are used to help invert for these unknowns. The results of performing a least squares inversion from our data points should manage to estimate our unknown parameters without too much error given that the data points used do not exceed unstable values (i.e. angles beyond the critical angle for a given impedance contrast of the two layers). For an overdetermined problem such as this, the matrix inversion may not yield perfect estimates of the unknowns. Therefore one approach into analyzing this problem is to try and find a unique solution. This is done by using the same number of equations, or data points, as there are unknown parameters.

### LEAST SQUARES IMPLEMENTATION

Two geological models were tested for the linear AVO inversion. Each of which were designed from parameters extracted from Russell et al. (2011). The two models in question are each composed of sand layers. The first geological model is described as a top sand that is gas saturated overlying a fully brine saturated sand. The second geological model consists of two fully brine saturated sands. The physical and fluid parameters that were used to forward model are illustrated in figure (2) where each parameter can be used to calculate a poroelastic property of the medium such as  $V_P$ ,  $V_S$ ,  $\rho$ ,  $f$ ,  $\mu$ , and etc. We will begin the

analysis with the first geological model that features a gas saturated sand overlying a fully brine saturated sand. It's corresponding AVO curves are produced in figure (3) where the input parameters taken from figure (2a) were used to plot each AVO curve. In order to test out one of the linear inversions, the Zoeppritz equations were replaced on the left hand side of equation (15) to act as synthetic data.

<p><b>Partially gas saturated sandstone for layer 1</b></p> <p><math>\kappa_{f1_0} = 0.195 \text{ GPa}</math>   <math>\kappa_{dry_0} = 3 \text{ GPa}</math>   <math>\kappa_{m_0} = 40 \text{ GPa}</math></p> <p><math>\rho_{w_0} = 1100 \text{ kg/m}^3</math>   <math>\rho_{gas_0} = 10 \text{ kg/m}^3</math>   <math>\rho_{sat_0} = 2235 \text{ kg/m}^3</math></p> <p><math>\rho_{m_0} = 2650 \text{ kg/m}^3</math>   <math>S_{w_0} = 90\%</math>   <math>S_{gas_0} = 10\%</math>   <math>\phi_0 = 25\%</math></p> <p><math>V_{P_0} = 1851 \text{ m/s}</math>   <math>V_{S_0} = 1159 \text{ m/s}</math>   <math>\mu_0 = 3 \text{ GPa}</math></p>	<p><b>Wet sandstone for layer 1</b></p> <p><math>\kappa_{f1_0} = 2.38 \text{ GPa}</math>   <math>\kappa_{dry_0} = 3 \text{ GPa}</math>   <math>\kappa_{m_0} = 40 \text{ GPa}</math></p> <p><math>\rho_{w_0} = 1100 \text{ kg/m}^3</math>   <math>\rho_{gas_0} = 10 \text{ kg/m}^3</math>   <math>\rho_{sat_0} = 2263 \text{ kg/m}^3</math></p> <p><math>\rho_{m_0} = 2650 \text{ kg/m}^3</math>   <math>S_{w_0} = 100\%</math>   <math>S_{gas_0} = 0\%</math>   <math>\phi_0 = 25\%</math></p> <p><math>V_{P_0} = 2489 \text{ m/s}</math>   <math>V_{S_0} = 1151 \text{ m/s}</math>   <math>\mu_0 = 3 \text{ GPa}</math></p>
<p><b>Wet sandstone for layer 2</b></p> <p><math>\kappa_{f1_1} = 2.38 \text{ GPa}</math>   <math>\kappa_{dry_1} = 3 \text{ GPa}</math>   <math>\kappa_{m_1} = 40 \text{ GPa}</math></p> <p><math>\rho_{w_1} = 1100 \text{ kg/m}^3</math>   <math>\rho_{gas_1} = 10 \text{ kg/m}^3</math>   <math>\rho_{sat_1} = 2262 \text{ kg/m}^3</math></p> <p><math>\rho_{m_1} = 2650 \text{ kg/m}^3</math>   <math>S_{w_1} = 100\%</math>   <math>S_{gas_1} = 0\%</math>   <math>\phi_1 = 25\%</math></p> <p><math>V_{P_1} = 2489 \text{ m/s}</math>   <math>V_{S_1} = 1152 \text{ m/s}</math>   <math>\mu_1 = 3 \text{ GPa}</math></p>	<p><b>Wet sandstone for layer 2</b></p> <p><math>\kappa_{f1_1} = 2.38 \text{ GPa}</math>   <math>\kappa_{dry_1} = 4.76 \text{ GPa}</math>   <math>\kappa_{m_1} = 40 \text{ GPa}</math></p> <p><math>\rho_{w_1} = 1100 \text{ kg/m}^3</math>   <math>\rho_{gas_1} = 10 \text{ kg/m}^3</math>   <math>\rho_{sat_1} = 2418 \text{ kg/m}^3</math></p> <p><math>\rho_{m_1} = 2650 \text{ kg/m}^3</math>   <math>S_{w_1} = 100\%</math>   <math>S_{gas_1} = 0\%</math>   <math>\phi_1 = 15\%</math></p> <p><math>V_{P_1} = 2923 \text{ m/s}</math>   <math>V_{S_1} = 1403 \text{ m/s}</math>   <math>\mu_1 = 4.76 \text{ GPa}</math></p>

FIG. 2: The two blocks on the left represent the first model and the right represents the second. Each model shows the input parameters that were used to calculate various poroelastic moduli. Note that the velocities shown include poroelastic properties so they are the saturated velocities.

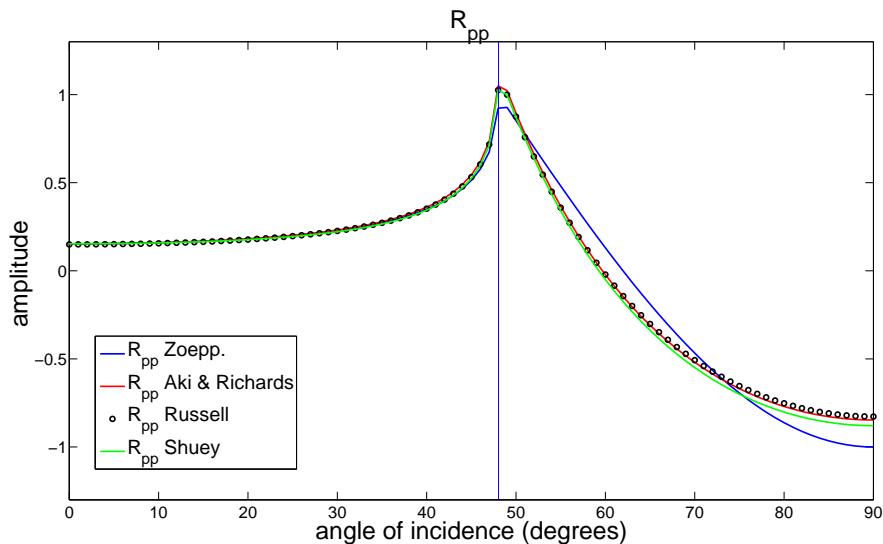


FIG. 3: For the first geological model, this figure represents the reflection coefficients (or amplitudes) as a function of the angle of incidence of a P-wave. The vertical blue line represents the critical angle at which the ray path of a P-wave does not reflect back to the surface. The amplitude values appearing before the blue line are real valued whereas the amplitudes appearing after the blue line have both real and imaginary components. For this particular geological model, the reflection coefficients have relatively the same value for small angles.

As seen before with the AVO equations shown by Aki and Richards (2002) and Russell et al. (2011), there are three unknown parameters. In order to find a unique solution for an overdetermined problem such as this, the same number of equations is chosen to solve for the unknown parameters i.e. three equations for three unknowns. Since we are more interested in the poroelastic properties of the subsurface, the equation provided by Russell et al. (2011) will be used to linearly invert for fluid, shear rigidity, and density. The way

in which this was performed, a series of inversions were performed on the synthetic data where a three equation arrangement involved the first data point located where the angle of incidence is zero, the second data point starting where the angle of incidence is 1 degree, and the third data point located just before the critical angle. This arrangement shows the first iteration of the series of inversions for a model. The next arrangement of equations would then involve the second data point to be located at an angle of incidence of 2 degrees where the first and last points remain static. And so on. This procedure is better represented in figure (4) where the magenta circles represent the static points and the teal circle represents an intermediate point, that increases in angle with each successive inversion. The known  $\frac{\Delta f}{f}$ ,  $\frac{\Delta \mu}{\mu}$ , and  $\frac{\Delta \rho}{\rho}$  for the first geological model are 1.657, 0.0, and 0.012 respectively. From the first iteration as seen in equation (16), the estimates for these reflectivities were 1.627, -0.036, and 0.059 respectively.

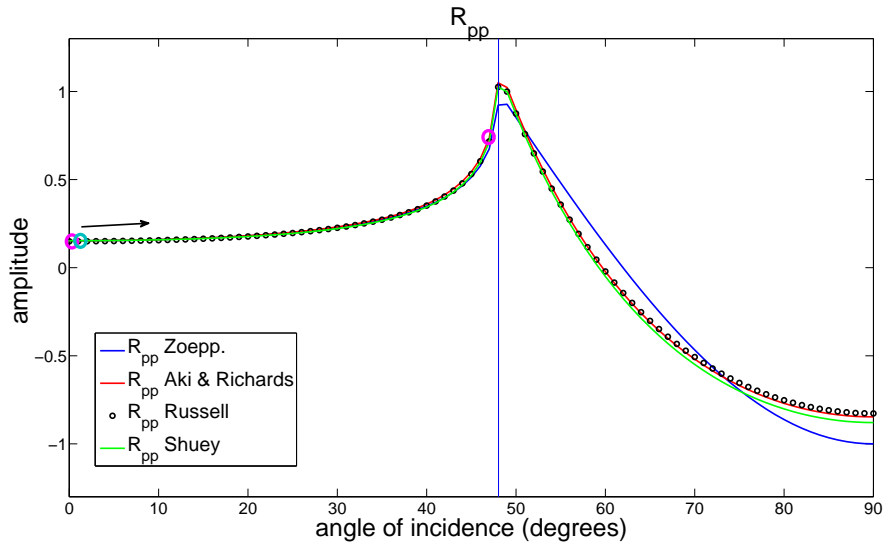


FIG. 4: This shows a graphical representation of how the three equations were selected for the parameter estimations. The magenta circles represent  $R_{PP}(\theta_1)$  and  $R_{PP}(\theta_{48})$  and the teal circle represents  $R_{PP}(\theta_2)$  in equation (16).

$$\begin{bmatrix} R_{PP}(\theta_1) \\ R_{PP}(\theta_2) \\ R_{PP}(\theta_{48}) \end{bmatrix} = \begin{bmatrix} c_1(\theta_1) & c_2(\theta_1) & c_3(\theta_1) \\ c_1(\theta_2) & c_2(\theta_2) & c_3(\theta_2) \\ c_1(\theta_{48}) & c_2(\theta_{48}) & c_3(\theta_{48}) \end{bmatrix} \begin{bmatrix} \frac{\Delta f_1}{f_1} \\ \frac{\Delta \mu_1}{\mu_1} \\ \frac{\Delta \rho_1}{\rho_1} \end{bmatrix} \quad (16)$$

For the first iteration of model 1, the first set of equations is shown in equation (16). This is similarly constructed for model 2 except that the third data point would be  $R_{PP}(\theta_{58})$  which can be seen in figure (7) where the critical angle is shown. Once a spectrum of f-m-r (fluid-mu-rho) values have been estimated, the bulk residual can show how accurate the inversion is working and can be expressed as

$$(r_{bulk})_i = \left[ \frac{\Delta f}{f} - \left( \frac{\Delta f}{f} \right)_{est} \right]_i + \left[ \frac{\Delta \mu}{\mu} - \left( \frac{\Delta \mu}{\mu} \right)_{est} \right]_i + \left[ \frac{\Delta \rho}{\rho} - \left( \frac{\Delta \rho}{\rho} \right)_{est} \right]_i \quad (17)$$

where  $i$  ranges from 1 to 48 for the case of model 1. A plot of the sum of the residuals between each reflectivity can be seen in figure (5)

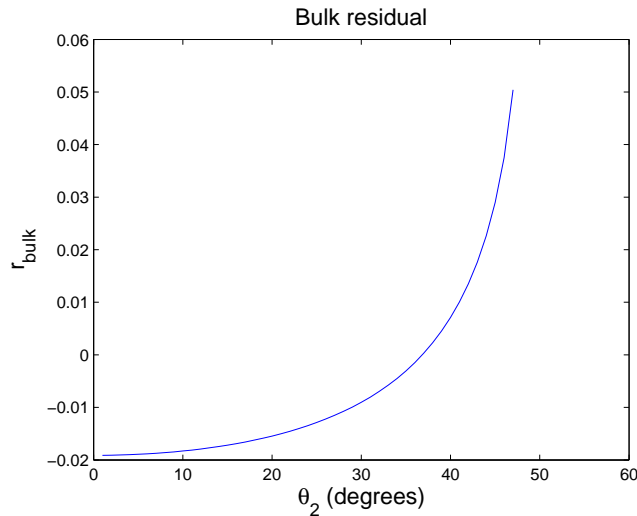


FIG. 5: The sum of the reflectivity residuals or bulk residual that illustrates the behaviour of the linear inversion results as  $\theta_2$  changes for model 1.

where we can see an increasing trend as the second equation gets larger. Since we are performing a linear least squares inversion, we would not expect to perfectly estimate the reflectivity terms but the bulk residual plot suggests that such an estimation has occurred when  $\theta_2$  is approximately 37 degrees. Although this is a peculiar result, a plot of the individual reflectivity residuals would show otherwise in figure (6) which shows that the sum of each reflectivity residual at  $\theta_2 = 37^\circ$  coincidentally sums to zero.

Analysis was similarly performed on the second geological model in which a brine saturated sand overlaid a brine saturated sand. The AVO curves are shown in figure (7) where all four curves seem to be behaving linearly from angles 0 to 40 as opposed to model 1 where the amplitudes are not behaving as such. We should therefore expect the linear inversion scheme to predict the reflectivities with a fair amount of stability and that not much variation in the bulk residual plot should occur. That is the case and is shown in figure (8) along with the plots of the individual reflectivity residuals in figure (9).

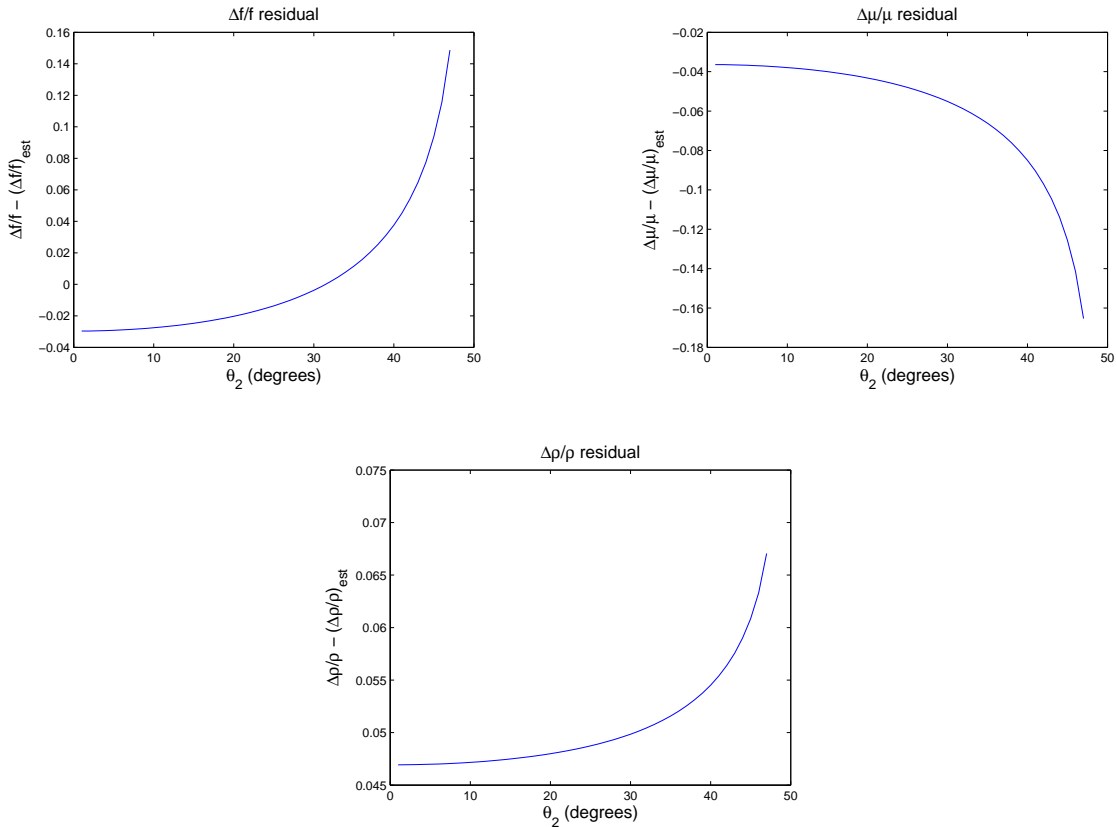


FIG. 6: Each panel represents the residuals of the true poroelastic terms (model true) and the inverted terms (model est) for model 1. In (6a) the estimation is exact when the intermediate equation was chosen at an angle of approximately 30 degrees. The other residuals however increase for both the  $\mu$  and  $\rho$  terms when the moving data point is at higher a higher angle. The sum of each curve reproduces the bulk residual curve in figure (5)

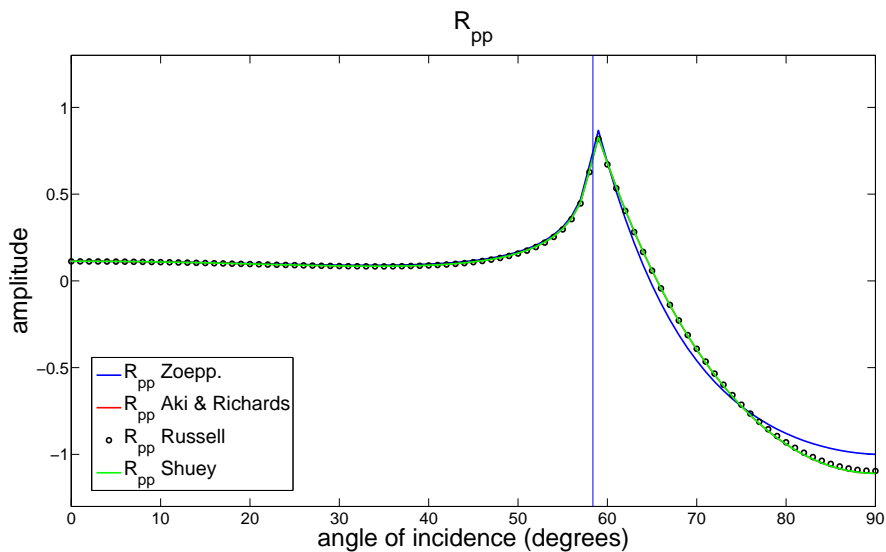


FIG. 7: For the second geological model, this figure represents the reflection coefficients (or amplitudes) as a function of the angle of incidence of a P-wave. The vertical blue line represents the critical angle at which the ray path of a P-wave does not reflect back to the surface. Similarly to the first model, the reflection coefficients for small angles have small variation. Note that the Aki and Richards approximation is located behind the Shuey approximation.

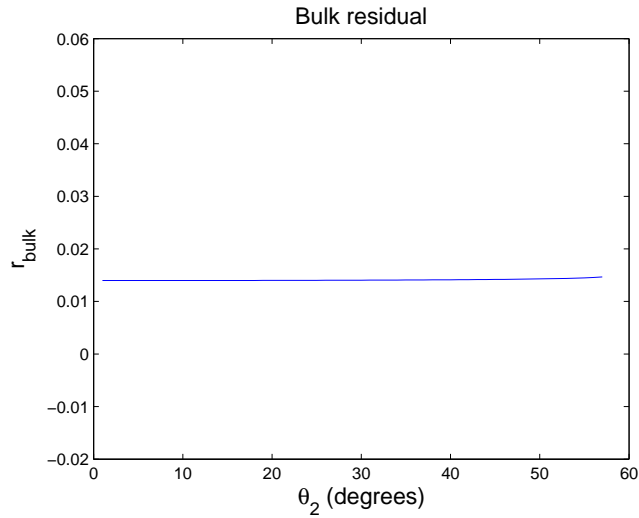


FIG. 8: The sum of the reflectivity residuals or bulk residual that illustrates the behaviour of the linear inversion results as  $\theta_2$  changes for model 2.

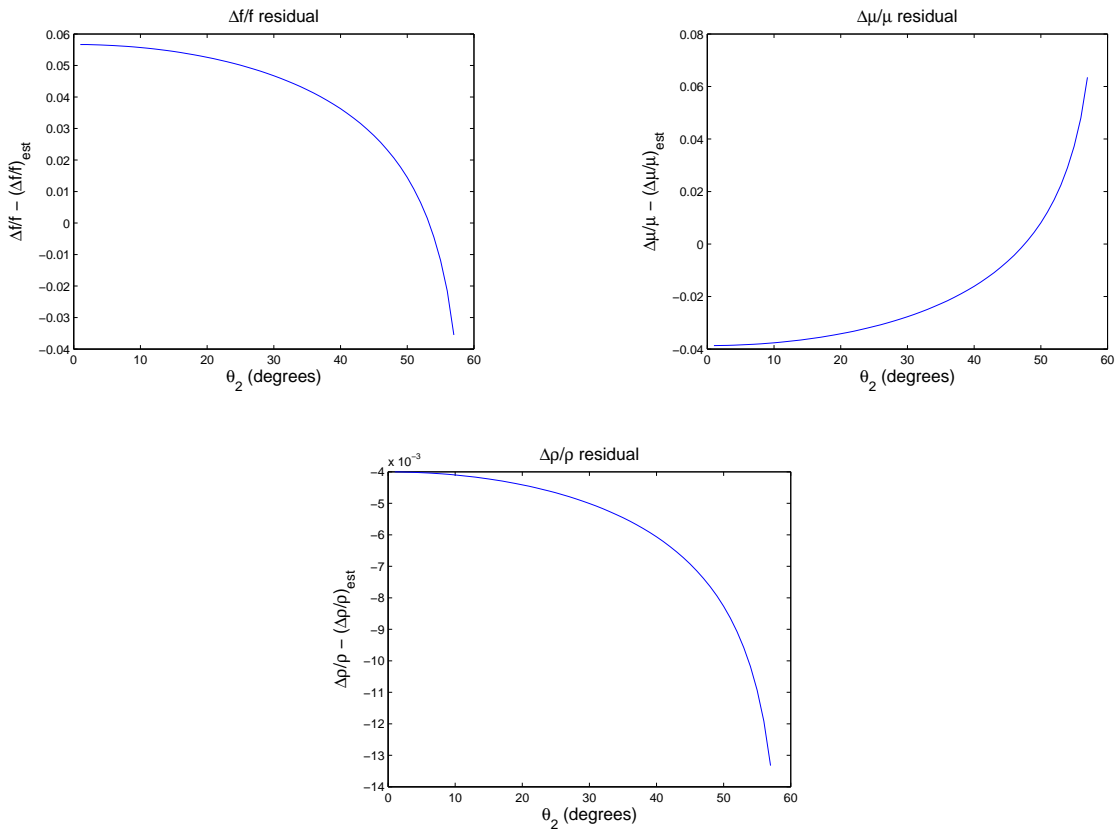


FIG. 9: The residual for the fluid term in (9a) predicts exactly the true model parameter at an angle of approximately 56 degrees for model 2. The shear modulus term in (9b) is also predicted exactly at an offset of approximately 50 degrees. The density term (9c) was not able to perfectly predict density for any incidence angle.

## EXACT POROELASTIC AVO: FORMULATION AND MODELING

Russell et al. (2011) use linearized forms for  $R_{PP}$  as a starting point for their analysis. One of our aims is to examine the role of nonlinearity in this parametrization. To that end here we will reformulate the full elastic Zoeppritz equations using the arguments made in that paper, and prepare them for expansion both linearly and with nonlinear corrections. Carrying out this expansion and inverting it to estimate the fluid parameter from reflection data will form the focus of our research in the coming year.

### Knott-Zoeppritz equations and solutions

Elsewhere in this report, Innanen (2011) discusses a matrix form for elastic displacement coefficients, including  $R_{PP}$ , originally due to Levin (1986) and Keys (1989). They are expressed in terms of an incident plane wave angle  $\theta$ , incidence medium (medium 0) P-wave and S-wave velocities and density, and target medium (medium 1) P-wave and S-wave velocities and density. Here we will express them as

$$\mathbf{P} \begin{bmatrix} R_{PP} \\ R_{PS} \\ T_{PP} \\ T_{PS} \end{bmatrix} = \mathbf{b}_P, \quad (18)$$

or

$$\begin{bmatrix} A_{11} & A_{12} & A_{13} & A_{14} \\ A_{21} & A_{22} & A_{23} & A_{24} \\ A_{31} & A_{32} & A_{33} & A_{34} \\ A_{41} & A_{42} & A_{43} & A_{44} \end{bmatrix} \begin{bmatrix} R_{PP} \\ R_{PS} \\ T_{PP} \\ T_{PS} \end{bmatrix} = \begin{bmatrix} b_1 \\ b_2 \\ b_3 \\ b_4 \end{bmatrix}, \quad (19)$$

where the elements of the first row are

$$\begin{aligned} A_{11} &= -\sin \theta, \\ A_{12} &= -\left[1 - \frac{1}{\gamma_{\text{sat}}^2} \sin^2 \theta\right]^{1/2}, \\ A_{13} &= \left(\frac{V_{P_1}}{V_{P_0}}\right) \sin \theta, \\ A_{14} &= \left[1 - \frac{1}{\gamma_{\text{sat}}^2} \left(\frac{V_{S_1}^2}{V_{S_0}^2}\right) \sin^2 \theta\right]^{1/2}, \end{aligned}$$

the elements of the second row are

$$\begin{aligned} A_{21} &= [1 - \sin^2 \theta]^{1/2}, \\ A_{22} &= -\frac{1}{\gamma_{\text{sat}}} \sin \theta, \end{aligned}$$

$$A_{23} = \left[ 1 - \frac{1}{\gamma_{\text{sat}}^2} \left( \frac{V_{P_1}^2}{V_{P_0}^2} \right) \sin^2 \theta \right]^{1/2},$$

$$A_{24} = -\frac{1}{\gamma_{\text{sat}}} \left( \frac{V_{S_1}}{V_{S_0}} \right) \sin \theta,$$

the elements of the third row are

$$A_{31} = 2 \left( \frac{1}{\gamma_{\text{sat}}^2} \right) \sin \theta [1 - \sin^2 \theta]^{1/2},$$

$$A_{32} = \frac{1}{\gamma_{\text{sat}}} \left[ 1 - 2 \left( \frac{1}{\gamma_{\text{sat}}^2} \right) \sin^2 \theta \right],$$

$$A_{33} = 2 \left( \frac{\rho_1}{\rho_0} \right) \left( \frac{V_{S_1}^2}{V_{S_0}^2} \right) \left( \frac{1}{\gamma_{\text{sat}}^2} \right) \sin \theta \left[ 1 - \left( \frac{V_{P_1}^2}{V_{P_0}^2} \right) \sin^2 \theta \right]^{1/2},$$

$$A_{34} = \left( \frac{\rho_1}{\rho_0} \right) \left( \frac{V_{S_1}}{V_{S_0}} \right) \left( \frac{1}{\gamma_{\text{sat}}} \right) \left[ 1 - 2 \left( \frac{V_{S_1}^2}{V_{S_0}^2} \right) \left( \frac{1}{\gamma_{\text{sat}}^2} \right) \sin^2 \theta \right],$$

the elements of the fourth row are

$$A_{41} = - \left[ 1 - 2 \left( \frac{1}{\gamma_{\text{sat}}^2} \right) \sin^2 \theta \right],$$

$$A_{42} = 2 \left( \frac{1}{\gamma_{\text{sat}}^2} \right) \sin \theta \left[ 1 - \left( \frac{1}{\gamma_{\text{sat}}^2} \right) \sin^2 \theta \right]^{1/2},$$

$$A_{43} = 2 \left( \frac{\rho_1}{\rho_0} \right) \left( \frac{V_{P_1}}{V_{P_0}} \right) \left[ 1 - 2 \left( \frac{V_{S_1}^2}{V_{S_0}^2} \right) \left( \frac{1}{\gamma_{\text{sat}}^2} \right) \sin^2 \theta \right],$$

$$A_{44} = -2 \left( \frac{\rho_1}{\rho_0} \right) \left( \frac{V_{S_1}^2}{V_{S_0}^2} \right) \left( \frac{1}{\gamma_{\text{sat}}^2} \right) \sin \theta \left[ 1 - \left( \frac{V_{S_1}^2}{V_{S_0}^2} \right) \left( \frac{1}{\gamma_{\text{sat}}^2} \right) \sin^2 \theta \right]^{1/2},$$

and the elements of vector on the right-hand side are

$$b_1 = \sin \theta,$$

$$b_2 = [1 - \sin^2 \theta]^{1/2},$$

$$b_3 = 2 \left( \frac{1}{\gamma_{\text{sat}}^2} \right) \sin \theta [1 - \sin^2 \theta]^{1/2},$$

$$b_4 = \left[ 1 - 2 \left( \frac{1}{\gamma_{\text{sat}}^2} \right) \sin^2 \theta \right].$$

Following Russell et al. (2011) we have used the term

$$\gamma_{\text{sat}} = \frac{V_{P_0}}{V_{S_0}} \quad (20)$$

to denote the *in situ*  $V_P/V_S$  ratio, in our case in the incidence medium. The subscript ‘sat’ indicates saturated, and will later serve to distinguish between rocks containing fluids and

‘dry’ rock frames. At the moment it just means the  $V_P/V_S$  ratio that is actually in the Earth, rather than any notional quantities relating to a rock model. As far as solutions go, our current interest is to focus on  $R_{PP}$ . To solve for this one element of the coefficient vector, we create a second matrix

$$\mathbf{P}_P \equiv \begin{bmatrix} b_1 & A_{12} & A_{13} & A_{14} \\ b_2 & A_{22} & A_{23} & A_{24} \\ b_3 & A_{32} & A_{33} & A_{34} \\ b_4 & A_{42} & A_{43} & A_{44} \end{bmatrix}, \quad (21)$$

in which case, by Cramer’s rule,

$$R_{PP} = \frac{\det \mathbf{P}_P}{\det \mathbf{P}}. \quad (22)$$

### Poroelasticity

The parameters of the target medium (medium 1) are the parameters of interest, being the unknowns in the AVO inverse problem. Notice that in the equations of the previous section these parameters only occur in terms of the three ratios

$$\left( \frac{V_{P1}}{V_{P0}} \right), \quad \left( \frac{V_{S1}}{V_{S0}} \right), \quad \text{and} \quad \left( \frac{\rho_1}{\rho_0} \right). \quad (23)$$

The poroelastic considerations of Russell et al. (2011) involve the breakup in particular of the bulk modulus into a ‘dry’ part and a ‘fluid’ part. Let us allow this breakup to influence the form of the three ratios above. In elastic media we have

$$V_P^2 = \frac{\kappa + (4/3)\mu}{\rho}, \quad (24)$$

and

$$V_S^2 = \frac{\mu}{\rho}. \quad (25)$$

In a poroelastic model we distinguish between the *in situ*, or saturated, parameters, e.g.,  $\rho_{\text{sat}}$  and  $\kappa_{\text{sat}}$ , and the parameters of the ‘dry’ rock frame supporting the fluid, e.g.,  $\rho_{\text{dry}}$  and  $\kappa_{\text{dry}}$ . The arguments of Biot and Gassmann are that  $\mu_{\text{sat}} = \mu_{\text{dry}}$ , but that the dry and saturated bulk moduli differ, leading to the poroelastic model of  $V_P$ :

$$V_P^2 = \frac{s + f}{\rho_{\text{sat}}}, \quad (26)$$

where

$$s = \kappa_{\text{dry}} + (4/3)\mu \quad (27)$$

is the skeleton (or rock frame) bulk modulus, and  $f$  is the fluid term discussed previously. This is suggestive that we consider two different  $\gamma$  terms:

$$\gamma_{\text{sat}} = \left( \frac{V_{P0}}{V_{S0}} \right)_{\text{sat}}, \quad \gamma_{\text{dry}} = \left( \frac{V_{P0}}{V_{S0}} \right)_{\text{dry}}. \quad (28)$$

## Alteration of the Zoeppritz equations

Let us now consider a poroelastic contrast in which across a plane boundary the parameters  $\mu_0, \rho_0, s_0$  and  $f_0$  undergo a contrast and become  $\mu_1, \rho_1, s_1$  and  $f_1$  (henceforth all densities,  $\rho_1, \rho_0$  etc. will refer to saturated, or *in situ* values). Russell et al. (2011) develop an expression for  $R_{pp}$  in terms of contrasts across a poroelastic boundary in  $f, \mu$ , and  $\rho$ . To that end we here define dimensionless perturbations

$$a_\mu = 1 - \frac{\mu_1}{\mu_0}, \quad a_\rho = 1 - \frac{\rho_1}{\rho_0}, \quad a_s = 1 - \frac{s_1}{s_0}, \quad a_f = 1 - \frac{f_1}{f_0}. \quad (29)$$

To manipulate these such that they fit into the matrix forms of the previous section, we point out first that

$$\left(\frac{\rho_1}{\rho_0}\right) = 1 - a_\rho, \quad (30)$$

and

$$\left(\frac{V_{S_1}^2}{V_{S_0}^2}\right) = \left(\frac{\mu_1}{\mu_0}\right) \left(\frac{\rho_0}{\rho_1}\right) = (1 - a_\mu)(1 - a_\rho)^{-1}. \quad (31)$$

The P-wave velocity ratio is more complex. In Appendix A we argue that if  $a_s \rightarrow 0$ , as in the forms of Russell et al. (2011), then

$$\left(\frac{V_{P_1}^2}{V_{P_0}^2}\right) = \left[1 - a_f \left(1 - \frac{\gamma_{dry}^2}{\gamma_{sat}^2}\right)\right] (1 - a_\rho)^{-1}. \quad (32)$$

By substituting equations (30)–(32) into equation (19) and forming the ratio in equation (22), we generate an exact expression for  $R_{pp}$  in terms of variations in  $f, \rho$ , and  $\mu$  across a poroelastic boundary.

## CONCLUSIONS

A series of three equation inversions were applied to the Zoeppritz equations using Russell's AVO linear approximation. The manner in which these inversions was performed was based on estimating three poroelastic properties from three different equations. These three equations were chosen where the first and last equations depicted the minimum and maximum value of the Zoeppritz derived AVO and the second equation would be a point in between. The optimally expected inversion result should be located where maximum coverage of the Zoeppritz curve occurs by the three equation arrangement. This was expected to be where the conditioning of the matrix inversion was greatest which would be where the second equation is located at maximum curvature of the Zoeppritz curve but was not the case. Typically in AVO inversion, using reflection coefficients at higher angles is not valid as the linearized approximations have more difficulty predicting those amplitudes. Thus data points at smaller angles are used instead of data found closer to the critical angle. With that, Russell et al. (2011) shows promising results in which the direct incorporation of fluid into AVO inversion provides a more comprehensive look into subsurface property behaviour. We propose an extension to Russell et al. (2011) by devising a non-linear AVO inversion scheme that may show differential benefit which will then be applied both theoretically and empirically.

## ACKNOWLEDGEMENTS

We would like to thank the sponsors of the CREWES project for their support, and to David Cho for his helpful comments and suggestions.

## REFERENCES

- Aki, K., and Richards, P. G., 2002, Quantitative seismology, 2nd ed.
- Berryman, J. G., 1999, Origin of gassmann's equations: Geophysics, **64**, 1627–1629.
- Biot, M. A., 1941, General theory of three-dimensional consolidation: Journal of Applied Physics, **12**.
- Gassmann, F., 1951, Über die elastizität poroser median: Vierteljahrsschrift der naturforschenden gesellschaft, **96**.
- Gray, D., Goodway, B., and Chen, T., 1999, Bridging the gap: Using avo to detect changes in fundamental elastic constants: 69th Annual International Meeting, 852–855.
- Innanen, K. A., 2011, A convenient matrix form for the knott-zoeppritz equations: CREWES Annual Report, **23**.
- Keys, R. G., 1989, Polarity reversals in reflections from layered media: Geophysics, **54**, 900–905.
- Levin, F., 1986, When reflection coefficients are zero: Geophysics, **51**, 736–741.
- Ostrander, W., 1984, Plane-wave reflection coefficients for gas sands at nonnormal angles of incidence: Geophysics, **49**, 1637–1648.
- Russell, B. H., Gray, D., and Hampson, D. P., 2011, Linearized avo and poroelasticity: Geophysics, **76**, C19–C29.
- Shuey, R., 1985, A simplification of the zoeppritz equations: Geophysics, **50**, 609–614.

## APPENDIX A

We begin by altering the ratio

$$\begin{aligned} \left( \frac{V_{P_1}^2}{V_{P_0}^2} \right) &= \left( \frac{s_1 + f_1}{\rho_1} \right) \times (V_{P_0}^2)^{-1} \\ &= \left( \frac{s_0 + f_1}{\rho_1} \right) \times (V_{P_0}^2)^{-1}, \end{aligned} \quad (\text{A-1})$$

to coincide with the case of no contrast in the dry rock bulk modulus  $s = \kappa_{\text{dry}} + \mu$ . This may then be re-expressed as

$$\begin{aligned} \left( \frac{V_{P_1}^2}{V_{P_0}^2} \right) &= \frac{s_0 + f_0 \times (f_1/f_0)}{\rho_0} \times \left( \frac{\rho_0}{\rho_1} \right) \times (V_{P_0}^2)^{-1} \\ &= \frac{s_0 + f_0 \times (1 - a_f)}{\rho_0} \times (1 - a_\rho)^{-1} \times (V_{P_0}^2)^{-1} \end{aligned} \quad (\text{A-2})$$

where in the last step we have used the definitions of the fluid and density perturbations. Continuing by invoking the definition of  $V_{P_0}^2$ ,

$$\begin{aligned} \left( \frac{V_{P_1}^2}{V_{P_0}^2} \right) &= \left[ \frac{s_0 + f_0}{\rho_0} - \frac{a_f f_0}{\rho_0} \right] \times (1 - a_\rho)^{-1} \times (V_{P_0}^2)^{-1} \\ &= \left[ 1 - a_f \frac{f_0}{f_0 + s_0} \right] (1 - a_\rho)^{-1}. \end{aligned} \quad (\text{A-3})$$

Finally, using the relations

$$\begin{aligned} f_0 &= \rho_0 V_{P_0}^2 - \gamma_{\text{dry}}^2 \rho_0 V_{S_0}^2 \\ s_0 &= \mu_0 \gamma_{\text{dry}}^2, \end{aligned} \quad (\text{A-4})$$

provided by Russell et al. (2011), we may re-write

$$\begin{aligned} \frac{f_0}{f_0 + s_0} &= \frac{\rho_0 V_{P_0}^2 - \gamma_{\text{dry}}^2 \rho_0 V_{S_0}^2}{\rho_0 V_{P_0}^2 - \gamma_{\text{dry}}^2 \rho_0 V_{S_0}^2 + \mu_0 \gamma_{\text{dry}}^2} \\ &= \frac{V_{P_0}^2 - \gamma_{\text{dry}}^2 V_{S_0}^2}{V_{P_0}^2 - \gamma_{\text{dry}}^2 V_{S_0}^2 + (\mu_0/\rho_0) \gamma_{\text{dry}}^2} \\ &= \frac{V_{P_0}^2 - \gamma_{\text{dry}}^2 V_{S_0}^2}{V_{P_0}^2 - \gamma_{\text{dry}}^2 V_{S_0}^2 + \gamma_{\text{dry}}^2 V_{S_0}^2} \\ &= \frac{V_{P_0}^2 - \gamma_{\text{dry}}^2 V_{S_0}^2}{V_{P_0}^2} \\ &= 1 - \frac{\gamma_{\text{dry}}^2}{\gamma_{\text{sat}}^2}. \end{aligned} \quad (\text{A-5})$$

Hence we have, finally,

$$\left( \frac{V_{P_1}^2}{V_{P_0}^2} \right) = \left[ 1 - a_f \left( 1 - \frac{\gamma_{\text{dry}}^2}{\gamma_{\text{sat}}^2} \right) \right] (1 - a_\rho)^{-1}. \quad (\text{A-6})$$